Optical response of excitonic polaritons in photonic crystals

S. Nojima
NTT Basic Research Laboratories, 3-1 Morinosato-Wakamiya, Atsugi, Kanagawa 243-0198, Japan
(Received 3 September 1998)

Nonlocal investigations are presented for exciton-photon coupling in photonic crystals consisting of two kinds of alternating slabs (CuCl/NaCl), for which excitons exist only in one (CuCl) of the two slabs. Studies are carried out for several typical combinations of period and slab thickness. The lower branch of the excitonic polariton for this system is found to split into many small bands separated by small band gaps (polariton gaps). This phenomenon is explained as the band splitting caused by the coherent interference of polaritonic waves in periodic systems. At the same time, the group velocity of light is greatly reduced in the presence of the excitons. The present nonlocal study demonstrates a double exciton-photon coupling, in which the upper branch of the polariton couples again with the size-quantized exciton states. A long-wavelength approximation is also presented along with a discussion of its validity for simplifying the nonlocal theory. The absorbance and reflectance spectra computed using the transfer matrices exactly reproduce the above small bands for the same systems. An examination of the coupling scheme among excitons, photons, and the structural periodicity indicates that the former two couple with each other more strongly than the other combinations of them. The exciton component of polariton, which is localized in each slab in darkness, could be construed as being delocalized with the assistance of the photon. [S0163-1829(99)05208-X]

I. INTRODUCTION

The optical properties of semiconductor microstructures have been the subject of intense investigations for a couple of decades.[1] Here the author wishes to classify the optical response of these structures from his own point of view. First, the system should be either (A) an isolated microstructure or (B) an assembly of microstructures. Second, the optical response must involve either (A′) the photons or (B′) the matter particles (or their elementary excitations) as well as the photons. Among the four possible combinations of these factors, two groups AA′ and AB′ are well known. A typical example of group AA′ is Mie scattering, where the light is scattered by a microstructure whose size is comparable to the wavelength of light. The other group AB′ has been extensively studied up to now. This model was frequently employed for analyzing optical devices that exploit microstructures as well as understanding their optical properties. In group AB′, most optical processes are treated as processes which could occur in an isolated microstructure (e.g., a single quantum well).[1] The optical response of the whole system (e.g., multiple quantum wells) is therefore obtained by simply summing up the responses of the individual structures.

What we call the photonic crystal seems to fall into group BA′. Photonic crystals,[2] which in recent years have attracted much attention, are periodic structures consisting of alternatingly arranged dielectric materials. They should therefore be regarded as special cases in group BA′, i.e., periodic assemblies of microstructures. In ordinary photonic environments made of uniform medium, the optical energy bands are no more than monotonic, i.e., linear and continuous. In contrast, with the photonic crystals, we may be able to obtain the desired photonic bands by properly designing the crystal structure. In particular, the photonic band gap—formed in a manner analogous to the electronic band gap in electronically periodic systems—could be useful in controlling the light in the medium, because it disallows the presence of optical modes in photonic crystal.[3] Considerable effort has been devoted to achieving usable photonic crystals experimentally, and to exploring theoretically such crystals with larger band gaps.[4]

It seems to the author, however, that the study of photonic crystals has so far focused on the formation of photonic bands and band gaps. Indeed, photonic crystal exhibits an unusual photon energy disperion, but this should be regarded as a space for light. For notable optoelectronic phenomena to occur in this space, there must be some other participants which act on the stage of this photonic dispersion. These other participants should be matter particles (electrons and holes)[5,6] or their elementary excitations (excitons).[7] The author thus believes that the photonic crystal should be considered as not only a space for light but also a stage for the physics of the optical properties of matter. This could be done, for example, by casting the above particles onto the stage, or the optical energy dispersion of photonic crystals. This is an intense motivation for studying the last group (BB′). One possible solution for this idea may exist in a regular arrangement of active media, which exhibits energy exchange between the matter and the photon systems through the electronic or excitonic transitions. In fact, some notable aspects may be anticipated for the optical responses of arranged active media when these structures are no longer isolated and some couplings between them can therefore be presumed. Several features arising from this cooperativity have been reported elsewhere.[7–9] The coherent interference of photons in an ordered system (ordinary photonic crystal) appears to give an impetus to the above study from a slightly different direction. At any rate, the participation of matter particles and their elementary excitations will undoubtedly

enrich the optical response in photonic crystals.

From this point of view, the author initiated the study of photonic crystals in which excitons exist at all lattice points.[7] Subsequently, in order to ascertain what would occur if gain media were employed instead at lattice points, we proposed[5,6] photonic crystals in which all lattice points are made of the same gain material embedded in other dissipative medium. Using those crystals, we clarified the enhancement[5] and polarization anisotropy[6] of optical gain. In the present paper, we extend previous study[7] of excitons in photonic crystals. Using the nonlocal exciton theory, we investigate the exciton-photon coupling (polariton effects) in one-dimensional photonic crystals. The purpose of this investigation is to isolate the kinetics of excitonic polaritons which may be exhibited in the whole system of regularly arranged microstructures.

II. THEORY

A. Nonlocal excitons in a slab

Excitons in a macroscopic-scale system must be treated using the nonlocal theory, because they spread throughout the whole solid with an appropriate dispersion.[10] This is true as long as we consider the systems larger than a very small system like a quantum well. Let us begin with the general Maxwell equation for electric field $\mathbf{E}(\mathbf{r})$ with space-dependent dielectric constant $\varepsilon(\mathbf{r})$ and exciton polarization:[11,12]

$$\nabla\times[\nabla\times\mathbf{E}(\mathbf{r})]=\left(\frac{\omega}{c}\right)^2\left[\varepsilon(\mathbf{r})\mathbf{E}(\mathbf{r})+4\pi\int d\mathbf{r}'\,\chi(\mathbf{r},\mathbf{r}')\mathbf{E}(\mathbf{r}')\right]. \tag{1}$$

The integral in this equation indicates the nonlocal exciton polarization. The nonlocal polarizability of exciton $\chi(\mathbf{r},\mathbf{r}')$ is

$$\chi(\mathbf{r},\mathbf{r}')=2\left(\frac{e}{m_0\omega}\right)^2|\mathbf{p}_{vc}|^2\sum_\lambda\frac{\psi_\lambda(0,\mathbf{r}')^*\psi_\lambda(0,\mathbf{r})}{\hbar\omega_\lambda-\hbar\omega-i\gamma}, \tag{2}$$

in the site representation, where only the resonant term is taken. Here, $\psi_\lambda(0,\mathbf{r})$ indicates an exciton wave function of state λ with the wave-function value at the origin for the internal motion of the exciton. In Eq. (2), $\mathbf{p}_{vc}$ is the momentum matrix element of the optical transition between the conduction and the valence bands,[13] and γ is the phenomenological damping factor. Ordinary notations are used for the other parameters.

Next, consider a slab with thickness d, which is located between the z coordinates of 0 and d with no bounds in the x and y directions. In order to obtain the equation for the light propagating in this slab (or a one-dimensionally modulated system) with an arbitrary in-plane wave-number vector, we assume for a while that this system has appropriate periods L_x and L_y in the x and y directions, respectively. Using the Bloch theorem in two dimensions, we next expand the electric field $\mathbf{E}(\mathbf{r})$ and dielectric constant $\varepsilon(\mathbf{r})$ into Fourier series, such that

$$\mathbf{E}(\mathbf{r})\equiv\mathbf{E}(\mathbf{r}_\parallel,z)=\sum_{\mathbf{G}_\parallel}\mathbf{E}(\mathbf{K}_\parallel+\mathbf{G}_\parallel,z)e^{i(\mathbf{K}_\parallel+\mathbf{G}_\parallel)\mathbf{r}_\parallel} \tag{3a}$$

and

$$\varepsilon(\mathbf{r})\equiv\varepsilon(\mathbf{r}_\parallel,z)=\sum_{\mathbf{G}_\parallel}\varepsilon(\mathbf{G}_\parallel,z)e^{i\mathbf{G}_\parallel\mathbf{r}_\parallel}. \tag{3b}$$

Here we introduce the in-plane wave-number vector $\mathbf{K}_\parallel$. Substituting Eq. (3) into Eq. (1) and taking the limit of the infinite L_x and L_y values, we obtain the Maxwell equation for the one-dimensionally modulated system:

$$\nabla\times[\nabla\times\mathbf{E}(\mathbf{K}_\parallel,z)]+i\mathbf{K}^0[\mathbf{e}\times(\nabla\times\mathbf{e})+\nabla\cdot\mathbf{e}-\mathbf{e}\cdot\nabla]\mathbf{E}(\mathbf{K}_\parallel,z)+\mathbf{K}^0(\mathbf{e}\cdot\mathbf{K}^0-\mathbf{K}^0\cdot\mathbf{e})\mathbf{E}(\mathbf{K}_\parallel,z)$$
$$=\left(\frac{\omega}{c}\right)^2\left[\varepsilon(0,z)\mathbf{E}(\mathbf{K}_\parallel,z)+4\pi S\int dz'\,\chi(\mathbf{K}_\parallel,z,z')\mathbf{E}(\mathbf{K}_\parallel,z')\right], \tag{4}$$

where $\mathbf{K}^0=(\mathbf{K}_\parallel,0)$. Here $\mathbf{e}$ is an identity vector operator, and it replaces itself by a vector that precedes or follows it like $(\mathbf{a}\times\mathbf{e})\mathbf{b}=\mathbf{a}\times\mathbf{b}$ and $\mathbf{a}(\mathbf{e}\cdot\mathbf{b})=\mathbf{a}\cdot\mathbf{b}$. Next, we assume for simplicity that the $1s$ exciton is confined within two hard walls on the both sides of the slab. This assumption corresponds to neglecting the dead layer effects near the walls, which arise from the finite size of the exciton. The wave function for the exciton in such a system is

$$\psi_\lambda(0,\mathbf{r})=\phi_{1s}(0)S^{-1/2}e^{i\mathbf{K}_\parallel\mathbf{r}_\parallel}\varphi_n(z), \tag{5a}$$

with

$$\varphi_n(z)=\left(\frac{2}{d}\right)^{1/2}\sin K_n z. \tag{5b}$$

In Eq. (5a), $\phi_{1s}(\boldsymbol{\rho})$ is the wave function of the internal motion of the $1s$ exciton, and $\varphi_n(z)$ describes the center-of-mass motion in the z direction. Here S is the area under consideration, and $K_n=(\pi/d)(n+1)$ is the size-quantized

wave number ($n=0,1,2,...$), and hence $|\lambda\rangle=|\mathbf{K}_\parallel,n\rangle$. Substituting Eq. (5) into Eq. (2) and replacing $\mathbf{K}_\parallel$ by $\mathbf{G}_\parallel$, we obtain

$$\chi(\mathbf{r}_\parallel,\mathbf{r}'_\parallel,z,z')=2\left(\frac{e}{m_0\omega}\right)^2|\mathbf{p}_{vc}|^2|\phi_{1s}(0)|^2S^{-1}\times\sum_{\mathbf{G}_\parallel,n}\frac{e^{i\mathbf{G}_\parallel(\mathbf{r}_\parallel-\mathbf{r}'_\parallel)}\varphi_n(z)\varphi_n(z')}{\hbar\omega_{\mathbf{G}_\parallel n}-\hbar\omega-i\gamma}. \quad (6a)$$

Here, $\mathbf{r}=(\mathbf{r}_\parallel,z)$, $\mathbf{r}'=(\mathbf{r}'_\parallel,z')$, and

$$\hbar\omega_{\mathbf{G}_\parallel n}=\hbar\omega_{1s}+\frac{\hbar^2G_\parallel^2}{2m}+\frac{\hbar^2K_n^2}{2\mu}, \quad (6b)$$

where $m=m_e+m_h$ and $\mu^{-1}=m_e^{-1}+m_h^{-1}$. Equation (6) can be rewritten as $\chi(\mathbf{r}_\parallel-\mathbf{r}'_\parallel,z,z')$. Its Fourier transform, which appears as the kernel of the integration in Eq. (4), becomes

$$\begin{aligned}\chi(K_\parallel,z,z')&=S^{-1}\int d(\mathbf{r}_\parallel-\mathbf{r}'_\parallel)\chi(\mathbf{r}_\parallel-\mathbf{r}'_\parallel,z,z')e^{-iK_\parallel(\mathbf{r}_\parallel-\mathbf{r}'_\parallel)}\\&=2\left(\frac{e}{m_0\omega}\right)^2|\mathbf{p}_{vc}|^2|\phi_{1s}(0)|^2S^{-1}\sum_{n=0}^{\infty}\frac{\varphi_n(z)\varphi_n(z')}{\hbar\omega_{K_\parallel n}-\hbar\omega-i\gamma}\\&=8\left(\frac{e}{\pi m_0\hbar\omega}\right)^2md|\mathbf{p}_{vc}|^2|\phi_{1s}(0)|^2S^{-1}\sum_{n=0}^{\infty}\frac{\sin\frac{\pi}{d}(n+1)z\sin\frac{\pi}{d}(n+1)z'}{(n+1)^2+a^2}, \quad (7a)\end{aligned}$$

with

$$a=\left(\frac{2m}{\hbar^2}\right)^{1/2}\frac{d}{\pi}\left(\hbar\omega_{1s}+\frac{\hbar^2K_\parallel^2}{2m}-\hbar\omega-i\gamma\right)^{1/2}. \quad (7b)$$

By analytically evaluating the series in Eq. (7) (see Appendix A), we obtain the final form of the nonlocal polarizability in one dimension:

$$\chi(\mathbf{K}_\parallel,z,z')=\left(\frac{e}{m_0\omega}\right)^2\frac{2m}{\hbar^2}|\mathbf{p}_{vc}|^2|\phi_{1s}(0)|^2S^{-1}\begin{cases}\dfrac{\cos q[d-(z+z')]-\cos q[d-|z-z'|]}{q\sin qd}, & :q\neq0\\ \dfrac{1}{2d}[2d-|z-z'|-(z+z')](-|z-z'|+z+z'), & :q=0,\end{cases} \quad (8a)$$

with

$$q=\left(\frac{2m}{\hbar^2}\right)^{1/2}\left(\hbar\omega-\hbar\omega_{1s}-\frac{\hbar^2K_\parallel^2}{2m}+i\gamma\right)^{1/2}. \quad (8b)$$

The coefficients in Eq. (8) can be rewritten in terms of the well-known relation

$$|\mathbf{p}_{vc}|^2|\phi_{1s}(0)|^2=\frac{\varepsilon_a m_0^2\omega_{1s}^2}{8\pi e^2}\Delta_{LT},$$

i.e., using the exciton-photon coupling constant Δ_{LT}. Equations (4) and (8) are convenient for calculating the light propagating in an arbitrary direction with wave-number vector $\mathbf{K}_\parallel$.

B. Excitons in a periodic structure

The schematic band diagram for the model of the one-dimensional periodic system is shown in Fig. 1, where an alternating layered structure consists of two different dielectric materials A and B. Here, we assume that material A is excitonically active, while material B is inactive in the photon energy region we are concerned about. As examples of materials A and B, we will take CuCl and NaCl, respectively, as will be discussed later (Sec. III A). Let the number of the layers be infinite, period l, and the slab A thickness d. We focus on the photon energy near the exciton resonance of material A. The excitons which might be created in the B slabs can therefore be neglected because of the pronounced energy separation. That is, it is sufficient to consider that excitons are present only in the A slab. Here we

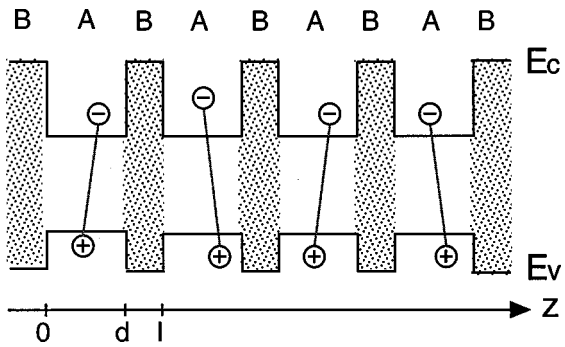

FIG. 1. Structure of a one-dimensional periodic system (photonic crystal) consisting of two different dielectric slabs A and B. Here, material A is excitonically active, and material B is inactive.

consider the A slabs to be thick enough to ensure that the scheme of the exciton center-of-mass quantization holds. Unnecessarily thick slabs, however, would make the exciton levels unseparable. Hence, in this study, we employ slabs with an appropriate thickness (see Sec. III A). With this structure, we must treat the excitons in it with nonlocal theory because of their spatial dispersion. The discussion in Sec. II A can therefore be applied to each A slab, i.e., the lattice point of this photonic crystal. When electromagnetic waves propagate in the direction (z axis) perpendicular to the layers, the x component of the electric field $E_x(z)$ has to satisfy the Maxwell equation

$$\frac{d^2E_x(z)}{dz^2}+\left(\frac{\omega}{c}\right)^2\left[\varepsilon(z)E_x(z)+4\pi S\int_{-\infty}^{\infty}dz'X(z,z')E_x(z')\right]=0. \tag{9}$$

For the electric field in the (excitonic) A slabs, we immediately obtain this equation by putting $K_\parallel=0$ into Eq. (4) and replacing $\varepsilon(0,z)$ and $\chi(z,z')$ by $\varepsilon(z)$ and $X(z,z')$, respectively. The integral in Eq. (9) is again the nonlocal exciton polarization [denoted by $P_x(z)$]. Since we now consider a periodic system, we have to assume some periodicity for the dielectric constant $\varepsilon(z)$ and the nonlocal polarizability $X(z,z')$. Here, we assume for simplicity that there are no direct interactions between excitons in different slabs. This implies that the exciton nonlocality works within each slab but does not extend to other slabs. In light of this assumption, we intuitively impose the following periodicity on $X(z,z')$. First, $X(z,z')$ must have a finite value when both z and z' are in the same A slab, while it must vanish for any other combinations of z and z' positions. That is,

$$X(z,z')=\begin{cases}\chi(z,z') & \text{for } z \text{ and } z' \text{ in the same cell}\\ 0 & \text{for any other } z \text{ and } z' \text{ positions,}\end{cases} \tag{10a}$$

where $\chi(z,z')$ is the nonlocal polarizability in one A slab. Second, once $\chi(z,z')$ is defined in a slab, it must have the same form in other slabs. This may be expressed by

$$\chi(z+nl,z'+nl)=\chi(z,z'), \tag{10b}$$

for $n=0,\pm1,\pm2,...$, etc.

Equation (9) is an integrodifferential equation with periodically varying coefficients. The ordinary procedure for an equation like this is to solve it using the Bloch theorem. To the author's knowledge, however, it does not always seem generic that the integrodifferential equation has a solution of the Bloch type. The group-theoretic approach to the integrodifferential operator can show it to be true indeed provided that the kernel possesses some kind of periodicity including the one in Eq. (10) (see Appendix B). Then, to confirm it in a practical problem, let us tentatively assume a solution of the Bloch type,

$$E_x(z)=\sum_G F_x(G)e^{i(G+K)z}, \tag{11}$$

where $F_x(z)$ is a periodic function with period l, and it is expanded into a Fourier series (G is the reciprocal lattice). The wave number K thus introduced describes the motion throughout the whole periodic structure, but this is not implied for motion in one slab. Substituting Eq. (11) into $P_x(z)$ [the integral in Eq. (9)], and using the periodicity of $\chi(z,z')$ defined above, we can show that

$$P_x(z)\equiv S\int_{-\infty}^{+\infty}dz'X(z,z')E_x(z')=Se^{iKml}\int_0^d du'\chi(u,u')E_x(u'), \tag{12}$$

for z and z' in slab A of the mth unit cell. Here, u and u' are intracell variables ($z=ml+u$ and $z'=ml+u'$ for $0<u,\ u'<d$). The function given by the second integral in Eq. (12) is therefore a cell-periodic function. As we can see in Eq. (12), the phase of the exciton polarization proceeds by Kl for unit translational operation ($m\rightarrow m+1$). We thus find that the exciton polarization $P_x(z)$ also has the form of the Bloch function. This appears to be physically correct, and reassures the existence of a Bloch-type solution for the integrodifferential equation with the kernel having the periodicity we imposed on the system. The next step in the calculation is the same as that for photonic crystals,[4] although it is more complicated in the present case because of the exciton term. We expand $\varepsilon(z)$ as

$$\varepsilon(z)=\sum_G \varepsilon(G)e^{iGz}, \tag{13a}$$

with

$$\varepsilon(G)=\varepsilon_b\delta_{G,0}+(\varepsilon_a-\varepsilon_b)fe^{-iGd/2}\frac{\sin Gd/2}{Gd/2}, \tag{13b}$$

where $f=d/l$ is the filling rate for slab A. Substituting Eqs. (11) and (13) into Eq. (9), we obtain the equation for the Fourier component $F_x(G)$:

$$F_x(G)(K+G)^2=\left(\frac{\omega}{c}\right)^2\sum_{G'}\left[\varepsilon(G-G')+4\pi X_f(G,G')\right]F_x(G'), \tag{14a}$$

with

$$X_f(G,G')=\frac{S}{l}\int_0^l\int_0^l du\,du'X(u,u')e^{iK(u'-u)+i(G'u'-Gu)}, \tag{14b}$$

Here, $X(u,u')$ is $\chi(u,u')$ for $0<u,\ u'<d$, while it vanishes elsewhere. Since $\chi(u,u')$ is given by Eq. (8) by making $K_\parallel=0$ and replacing z and z' by u and u', respectively, we can express $X_f(G,G')$ in an analytical form (not shown here because it is too long). The matrix to be diagonalized is

$$M(G,G')=(K+G)^2\delta_{G,G'}-\left(\frac{\omega}{c}\right)^2\left[\varepsilon(G-G')+4\pi X_f(G,G')\right]. \tag{15}$$

It is easy to show, using the analytical expression of $X_f(G,G')$, that the matrix M is Hermitian, and hence it gives real eigenvalues as long as $\gamma=0$. Since this matrix is a

function of ω and K, the eigenvalue problem cannot be solved using standard computer software. Accordingly, we determine the eigenvalues by searching the zeros of the determinant for matrix M defined above.

C. Long-wavelength approximation

The discussion presented in Sec. II B is somewhat complicated because of the correct nonlocal treatment for the exciton. In the long-wavelength region, this complexity can be reduced to a certain degree. In this subsection, we describe a method for simplifying the calculation. First, we consider the situation in which the A slabs are so thin that the electric field can be regarded as constant in each, i.e., $d \ll \lambda$, where λ is the wavelength of light. This does not imply the uniformity of the electric field throughout the photonic crystal, but it may differ for different slabs. Second, the exciton Bohr radius a_b is assumed to be much smaller than the slab thickness d, and therefore the nonlocal treatment is still necessary, i.e., $a_b \ll d < l$. The situation satisfying the above requirements simultaneously, i.e.,

$$a_b \ll d < l \ll \lambda \tag{16}$$

could be realized by carefully selecting the structures. The actual discussion of the structural parameters will be given in Sec. III A.

Let us rewrite the nonlocal polarizability of the exciton [making $K_\parallel = 0$ in Eq. (7)] in the form

$$\chi(z,z') = S^{-1} \sum_n c_n \varphi_n(z) \varphi_n(z'), \tag{17a}$$

where

$$c_n = 2\left(\frac{e}{m_0 \omega}\right)^2 \frac{|\mathbf{p}_{vc}|^2 |\phi_{1s}(0)|^2}{\hbar\omega_{0,n} - \hbar\omega - i\gamma}. \tag{17b}$$

The polarization in slab A of the mth cell is written as

$$P_x(z) = \sum_n c_n \varphi_n(z) \int_{m\text{th slab}} dz' \varphi_n(z') E_x(z'), \tag{18a}$$

where z is in the mth slab, and hence the integration in Eq. (18a) is carried out within the mth slab. Under the conditions given by Eq. (16), we can assume that the electric field is nearly constant in this slab. Therefore, the $E_x(z')$ term can be factored out as $E_x(z_m)$ from the integration in Eq. (18a),

$$\begin{aligned} P_x(z) &\cong \sum_n c_n \varphi_n(z) E_x(z_m) \int_{m\text{th slab}} dz' \varphi_n(z') \\ &\cong \chi_{\text{eff}}(z) E_x(z), \end{aligned} \tag{18b}$$

where z_m implies an appropriate position in the mth slab, but it just means the cell address since the electric field is uniform in this slab. Moreover, in the second equality of Eq. (18b), the $E_x(z_m)$ term is factored out from the summation, since it does not depend on n. This electric field is denoted $E_x(z)$, and the z dependence is recovered to show that it varies from one slab to another in the whole photonic crystal. Here we introduce the effective polarizability by

$$\chi_{\text{eff}}(z) = \sum_n c_n \varphi_n(z) \int_{m\text{th slab}} dz' \varphi_n(z'). \tag{19a}$$

What we immediately know from Eq. (19a) is that the spatial variation of the effective polarizability is described by the exciton wave function, and its intensity is determined by the integrated value for the exciton wave function in the slab:

$$\int_0^d du' \varphi_n(u') = \begin{cases} \dfrac{\sqrt{8d}}{\pi(n+1)} & \text{for even } n \\ 0 & \text{for odd } n, \end{cases} \tag{19b}$$

where the integral in the mth slab is converted to the one in the unit cell by $z' = ml + u'$. From this selection rule, we obtain

$$\chi_{\text{eff}}(z) = \left(\frac{4ed}{m_0 \hbar}\right)^2 \frac{|\mathbf{p}_{vc}|^2 |\phi_{1s}(0)|^2 m}{\pi^3 \omega^2} H_b\left(\frac{\pi}{d} u\right), \tag{20a}$$

where $H_b(x)$ is defined by

$$H_b(x) = \sum_{n=0,2,\ldots}^{\infty} \frac{\sin(n+1)x}{[(n+1)^2 + b^2](n+1)}, \tag{20b}$$

with

$$b = \left(\frac{2m}{\hbar^2}\right)^{1/2} \frac{d}{\pi} (\hbar\omega_{1s} - \hbar\omega - i\gamma)^{1/2}, \tag{20c}$$

where $z = ml + u$, and the summation must be carried out for even n. The summation given by Eq. (20b) can be expressed as the analytical form

$$H_b(x) = \frac{\pi}{4b^2}\left[1 - \frac{2\sinh b(\pi - x)}{\sinh b\pi} + \frac{\sinh b(\pi/2 - x)}{\sinh b\pi/2}\right], \tag{21}$$

where $x = (\pi/d)u = (\pi/d)(z - ml)$. (See Appendix A for an evaluation of this summation.) Using this polarizability, the Maxwell equation is shown to become the simple form

$$\frac{d^2 E_x(z)}{dz^2} + \left(\frac{\omega}{c}\right)^2 [\varepsilon(z) + 4\pi X_{\text{eff}}(z)] E_x(z) = 0, \tag{22}$$

which is an ordinary differential equation. Here $X_{\text{eff}}(z)$ is $\chi_{\text{eff}}(z)$ given by Eq. (20a) in slab A, while it vanishes in slab B. However, since $\chi_{\text{eff}}(z)$ is still a function of ω, Eq. (22) has to be solved by calculating the determinant for the relevant matrix, as discussed in Sec. II B.

D. Optical response

Since the exciton polarization obtained in Sec. II B indicates the response of the system to the external light field, the optical absorption could be calculated by the same nonlocal approach. However, the exciton polarization is a function of the position because of the nonlocal nature of the treatment. This makes it difficult to calculate the optical response (e.g., absorption), which is in contrast to the local system in which the polarization depends upon the photon energy but not upon the position. The convenient quantity defined in the local system, such as the absorption coeffi-

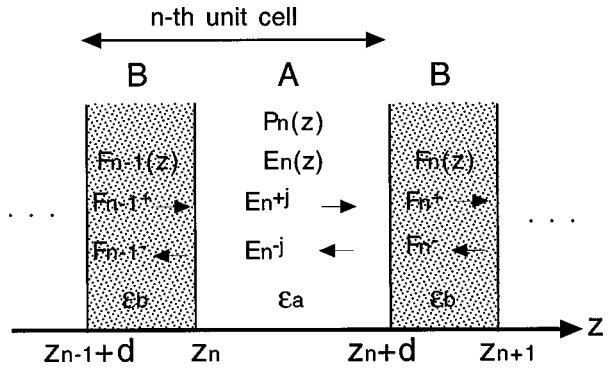

FIG. 2. Schematic picture of light propagating in the vicinity of the nth unit cell. Here, the system consists of groups (BA) (BA)...(BA)B, i.e., N unit (BA) cells plus an extra B layer, sandwiched between the air.

cient, therefore becomes meaningless in the nonlocal systems. In light of the above, here we calculate the optical response of the periodic systems in terms of tranfer matrices. This is a primitive but straightforward approach, and therefore it will also help to confirm the other more elaborate approach in the preceding subsections, i.e., to solve the integrodifferential equation.

Let us consider a periodic system like the one in Fig. 1, except that it has a finite number (N) of A slabs. Figure 2 shows the schematic picture for the light propagating in the vicinity of the nth unit cell, where the normal incidence to the interface is employed. Here, we assume the group (BA)(BA)...(BA)B structure, i.e., N unit (BA) cells plus an extra B layer, sandwiched between the air. Let the B-A interface in the nth unit cell have the coordinate $z=z_n=(n-1)l$ for $n=1,2,...,N$. Therefore, the far left interface between the air and layer B has the coordinate $z=-(l-d)$, and the far right one between layer B and the air has $z=Nl$. First, the electric fields outside the system (i.e., in the air) have the form

$$F_{\text{left}}(z)=F_i e^{iq_0(z+l-d)}+F_r e^{iq_0(d-l-z)} \tag{23a}$$

at the left end with the amplitudes for the incident (F_i) and reflected (F_r) waves, and

$$F_{\text{right}}(z)=F_t e^{iq_0(z-Nl)} \tag{23b}$$

at the right end with the amplitude for the transmitted wave (F_t). Here $q_0=\omega/c$. In layer B, the field $F_{n-1}(z)$ in the nth unit cell is

$$F_{n-1}(z)=F_{n-1}^{+}e^{iq_b(z-z_{n-1}-d)}+F_{n-1}^{-}e^{iq_b(z_n-z)}, \tag{24}$$

where $q_b=\sqrt{\varepsilon_b}(\omega/c)$ is the wave number of light in layer B, and F_{n-1}^{+} and F_{n-1}^{-} indicate the amplitudes of waves propagating in the opposite directions. While $F_{n-1}(z)$ is defined for $n=1,2,...,N$, let $F_N(z)$ be the field in the extra B layer furthest to the right. Since slab A is excitonic, the electric field $E_n(z)$ in the nth slab A consists of the two components arising from the two polariton branches,

$$E_n(z)=\sum_{j=1}^{2}\left[E_n^{+j}e^{iQ_j(z-z_n)}+E_n^{-j}e^{iQ_j(z_n+d-z)}\right], \tag{25}$$

where E_n^{+j} and E_n^{-j} are the amplitudes of the electric field propagating forward and backward, respectively, for the j polariton branch ($j=1,2$). Here Q_j is the wave number of the bulk polariton, such that

$$Q_j=\frac{1}{\sqrt{2}}[q^2+q_a^2+(-)^j\{(q^2-q_a^2)^2+4B\}^{1/2}]^{1/2}.$$

Here, the parameters in Q_j are $q_a=\sqrt{\varepsilon_a}(\omega/c)$, and

$$q=\left(\frac{2m}{\hbar^2}\right)^{1/2}(\hbar\omega-\hbar\omega_{1s}+i\gamma)^{1/2},$$

$$B=2m\varepsilon_a\left(\frac{\omega_{1s}}{\hbar c}\right)^2\Delta_{\text{LT}}.$$

Using the electric fields defined above, the exciton polarization in slab A of the nth unit cell is expressed as[12]

$$P_n(z)=B\sum_{j=1}^{2}\frac{E_n^{+j}e^{iQ_j(z-z_n)}+E_n^{-j}e^{iQ_j(z_n+d-z)}}{Q_j^2-q^2}. \tag{26}$$

The electric fields in each layer can be connected to those in the neighboring layers using the Maxwell boundary conditions (MBC's):

$$F_{n-1}(z_n)=E_n(z_n) \quad \text{and} \quad F'_{n-1}(z_n)=E'_n(z_n) \tag{27a}$$

at the left interface of slab A ($z=z_n$), and

$$E_n(z_n+d)=F_n(z_n+d)$$

and

$$E'_n(z_n+d)=F'_n(z_n+d) \tag{27b}$$

at the right interface of slab A ($z=z_n+d$). These four conditions are insufficient for determining the six coefficients in Eqs. (24) and (25); two more conditions are needed to determine all of them. These are known as additional boundary conditions (ABC's), which arise from the two polariton modes in slab A.[14] The assumption mentioned before for neglecting the dead layer [Eq. (5)] gives what is called the Pekar's boundary conditions,[14] i.e., the simplest form of the ABC's. They require that the polarization vanishes at the surface of slab A, such that

$$P_n(z_n)=0 \quad \text{and} \quad P_n(z_n+d)=0. \tag{28}$$

The transfer matrix between the amplitudes $(F_{n-1}^{+},F_{n-1}^{-})$ in layer B and those (F_n^{+},F_n^{-}) in its neighboring B layer is thus uniquely determined. Next, by using the MBC's to connect $F_{\text{left}}(z)$ to $F_0(z)$, and to connect $F_N(z)$ to $F_{\text{right}}(z)$,

$$F_{\text{left}}(d-l)=F_0(d-l),$$

$$F'_{\text{left}}(d-l)=F'_0(d-l),$$

$$F_N(Nl)=F_{\text{right}}(Nl),$$

and

$$F'_N(Nl)=F'_{\text{right}}(Nl),$$

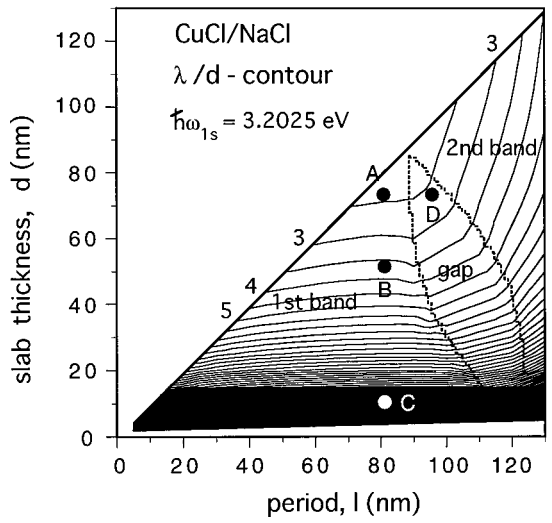

FIG. 3. Contour lines of the λ/d ratio for a variety of combinations of l and d values at a fixed CuCl exciton resonance $\hbar\omega_{1s}=3.2025$ eV. Here $\lambda=2\pi/K$, where K is the wave number at $\hbar\omega_{1s}$ in the photonic band. The numbers indicate the λ/d ratios for the corresponding line. Samples studied in this paper are denoted A, B, C, and D.

we obtain the relations among the amplitudes in the air (F_i, F_r, and F_t):

$$\begin{pmatrix} F_i \\ F_r \end{pmatrix} = (M_t^N M_s)^{-1} M_g F_t . \tag{29}$$

Matrices M_s, M_t, and M_g indicate the transfer matrices from the air to layer B at the left end, from layer B via layer A to layer B, and from layer B to the air at the right end, respectively. The explicit forms of matrices are given in Appendix C. Reflectance R and transmittance T can be calculated by

$$R=\left|\frac{F_r}{F_i}\right|^2 \quad \text{and} \quad T=\left|\frac{F_t}{F_i}\right|^2, \tag{30}$$

using Eq. (29). The absorbance A is given by $A=1-R-T$.

III. RESULTS

A. Selection of structures

In practical calculations, we employ the periodic system consisting of CuCl as slab A and NaCl as slab B. This is because CuCl exhibits a strong exciton-photon coupling, and the band gaps of these materials are energetically well separated. The importance of the nonlocal treatment for the exciton is determined by how strongly the light field varies in the region where excitons exist. We therefore introduce the ratio λ/d as a measure of the effectiveness for treating excitons nonlocally (λ is the wavelength, and d the CuCl slab thickness). Evidently, the smaller λ/d ratio augments the importance of the nonlocal treatment, while the larger λ/d ratio diminishes it and permits the long-wavelength approximation. Figure 3 displays the contour lines of the λ/d ratio for a variety of combinations of l and d values at a fixed CuCl exciton resonance $\hbar\omega_{1s}=3.2025$ eV. For given l and d values, we can immediately obtain the photonic band structure (neglecting exciton effects). Next we determine K from the point at which the level $\hbar\omega=\hbar\omega_{1s}$ intersects with the photonic band, and therefore $\lambda=2\pi/K$ at this point. Naturally, only the lower-right half-plane ($d<l$) has meaning. The numbers in Fig. 3 indicate the λ/d ratios for the corresponding lines. This diagram can be divided into three regions depending on whether the exciton resonance locates in the first band, in the second band, or within the photonic band gap. The bottom area in this diagram gives a very high λ/d ratio, allowing the long-wavelength approximation, while the area close to the straight line ($d=l$) gives a low ratio, which means the nonlocal treatment of excitons is required. Among the possible combinations of l and d, we select four samples (A, B, C, and D) to study the polariton effects in detail in this paper. Sample A is selected because it is a typical one where nonlocal effects are important; sample B because it is at an intermediate point between samples A and C in Fig. 3; sample C because the long-wavelength approximation may be possible for this sample; and sample D because the exciton resonance is located within the photonic band gap. The (l,d) values in nm and λ/d ratios are (81.3, 73.1) 2.4 for sample A, (81.3, 51.0) 3.7 for sample B, (81.3, 10.0) 23 for sample C, and (95.5, 73.1) 2.6 for sample D. Other parameters used are the mass and the resonance of a CuCl exciton, which are $m=2.5m_0$ and $\hbar\omega_{1s}=3.2025$ eV, respectively; the dielectric constants, which are $\varepsilon_a=5.00$ for CuCl and $\varepsilon_b=2.46$ for NaCl; and the exciton-photon coupling constant, which is $\Delta_{\mathrm{LT}}=5.5$ meV. We set the damping factor γ to 0 for calculating the polariton dispersions. For the calculation of optical responses, we used γ of 0.001 meV.

B. Polariton dispersions

The correct nonlocal calculations were carried out using the formulation in Sec. II B to obtain the energy dispersions of excitonic polaritons in photonic crystals. Figures 4, 5, 6, and 7 correspond to samples A, B, C, and D, respectively. In all figures in this paper, the ω and K values are normalized in the unit of $2\pi c/l$ and $2\pi/l$, respectively. Prior to mentioning the details of polariton dispersions, we should ascertain where the exciton resonance is located in the photonic band. Here the term ''photonic band'' implies the band obtained by neglecting the exciton effects (i.e., using $\varepsilon_a=5.00$ and neglecting the frequency-dependent part in the dielectric constant of CuCl). The insets show the photonic bands (solid lines) together with the exciton resonance ω_{1s} location (dotted line). The band gap produced (shaded area) separates the photonic band into the first and second bands. While the exciton resonance for samples A, B, and C is close to the top of the first photonic band, it exists within the photonic band gap for sample D.

We now turn our attention to the energy dispersions of the excitonic polaritons. Among these figures, Fig. 4 covers the widest energy range. Since we are interested in the energy region near the exciton resonance, the ordinate of the upper graph in Fig. 4 is magnified in the vicinity of the resonance. The lower graph is, conversely, scaled down to cover a wider energy range than in the upper one and the two are joined together continuously. Other figures depict only the vicinity of the exciton resonance. The steep vertical line (dashed line)

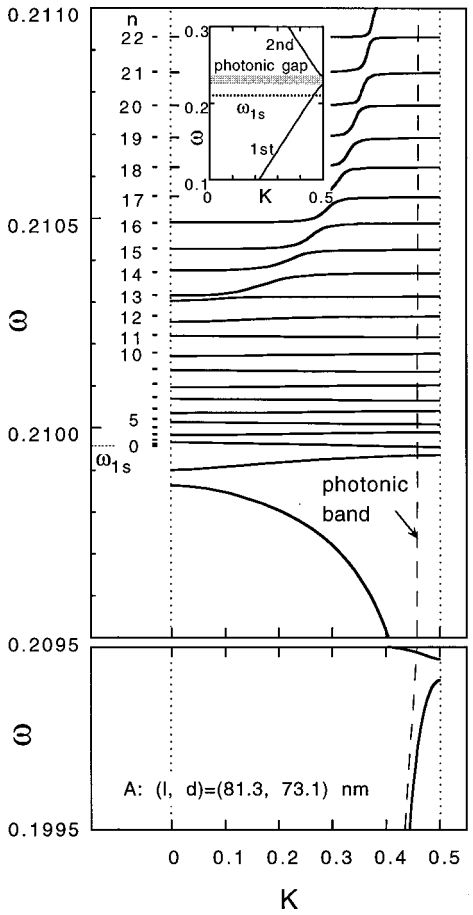

FIG. 4. Polariton dispersion for sample A. Here, and in Figs. 5, 6, and 7, locations of size-quantized exciton levels are indicated by bars together with their index n. The inset shows the dispersion of the photonic crystal (i.e., neglecting the exciton effects) and the location of the exciton resonance ω_{1s}. In all figures in this paper, ω and K are normalized by $2\pi c/l$ and $2\pi/l$, respectively.

for samples A, B, and C is the photonic band (i.e., exciton effects are neglected), which is identical to the first band in the inset. For sample D, the dashed line (the real part of the complex wave number) is at the Brillouin-zone (BZ) edge, indicating that this energy region is within the photonic band gap. With exciton-photon coupling, the monotonic energy dispersion (dashed line) of the photonic crystal is found to split into many small bands separated by small band gaps. Note that these bands are dispersive, i.e., giving finite group velocities (see Sec. IV A). In the higher-energy region for samples A, B, and D, and in the whole energy region for sample C, we observe the anticrossing of the dispersion curves, i.e., the two curves approach one another and then move apart due to the repulsion between them. The band energy values in the higher-energy region for samples A, B, and D coincide well with the size-quantized exciton levels, the positions of which are indicated by bars together with their index n. This coincidence, however, gradually declines with decreasing energy. In the lower-energy region, there is evidently no correspondence between them. In contrast, every band energy of sample C reproduces the size-quantized exciton level. Finally, note that real polariton dispersions are observed for sample D, despite the fact that the exciton resonance is within an energy region which would disallow optical modes in the absence of excitons.

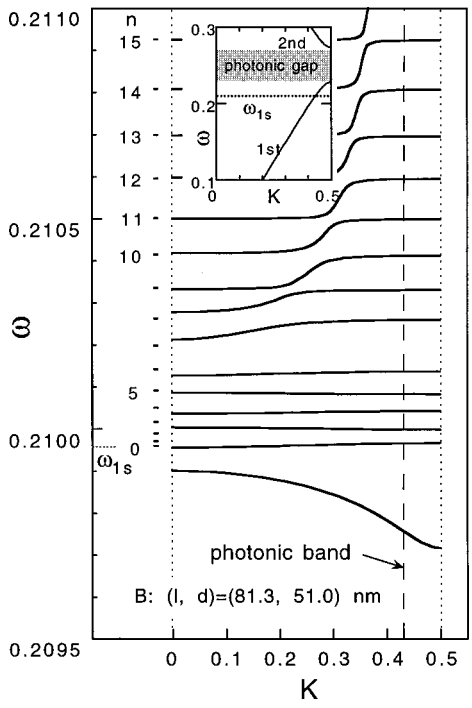

FIG. 5. Polariton dispersion for sample B.

IV. DISCUSSION

In this section, on the basis of the polariton dispersions obtained in Sec. III, we extend the investigation in order to elucidate the kinetics of polaritons in photonic crystals. The points covered in the following discussion are (1) the relation between the nonlocal behavior in periodic systems and the bulk materials' nonlocality with the focus on samples A and B, (2) the possibility of long-wavelength approximation for

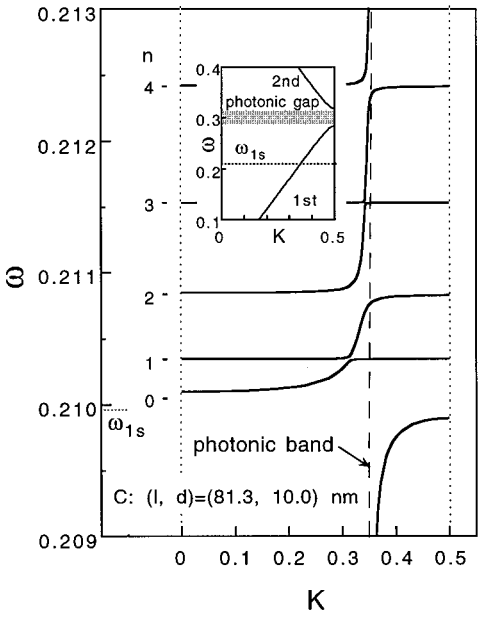

FIG. 6. Polariton dispersion for sample C.

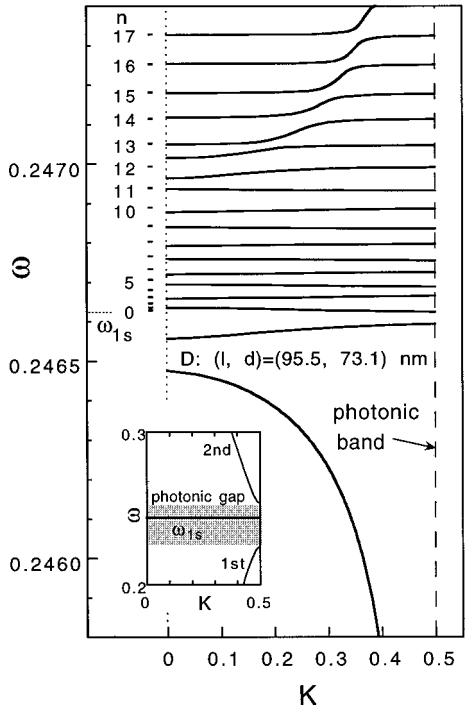

FIG. 7. Polariton dispersion for sample D.

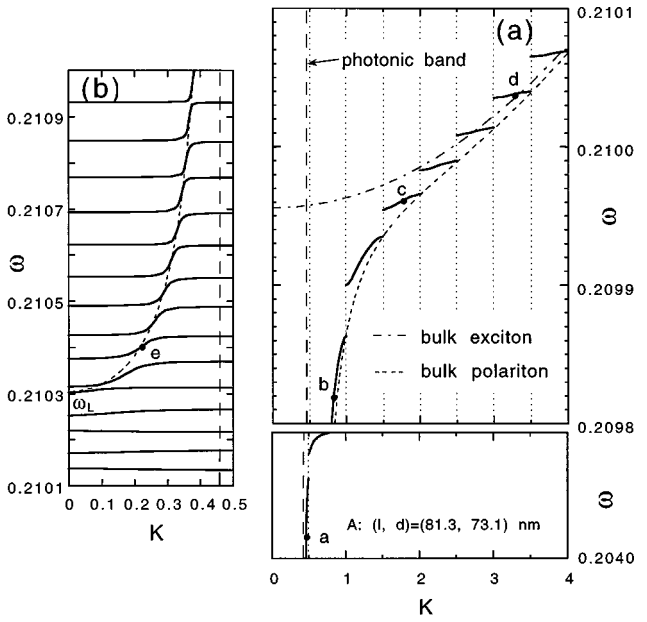

FIG. 8. Polariton dispersion replotted from Fig. 4, and magnified in the vicinity of the exciton resonance. (a) Dispersion expanded into the extended K zone at lower energies, and (b) dispersion redrawn in the first Brillouin zone at higher energies. Bulk polariton dispersions using the renormalized exciton mass are shown by broken lines in both (a) and (b).

samples A and C, and (3) the optical responses of systems in which the exciton resonance is in the photonic band (sample A) and in the photonic band gap (sample D). We regard sample A as the primary object for the present study and consider the others as references.

A. Extension to higher-order zones

In order to clarify what happens to the energy dispersion in periodic structures when there is exciton-photon coupling, we expanded the polariton dispersion near the resonance for sample A into the extended K zone up to the eighth BZ [see Fig. 8(a)]. The upper graph in Fig. 8(a) is more magnified than the lower one. The mutual arrangement of the small bands in this figure (solid lines) reminds us of the splitting of the electronic bands in what we call semiconductor superlattices.[15] In light of this, we attempted to account for the formation of these small bands in Fig. 8(a). The polariton dispersion ω_{bK} in bulk CuCl material is ordinarily obtained by solving the equation[16]

$$\left(\frac{cK}{\omega_{bK}}\right)^2=\varepsilon_{\rm pc}+\left(\frac{\varepsilon_a\Delta_{\rm LT}}{\hbar\omega_{1s0}}\right)\frac{\omega_{1sK}}{\omega_{1sK}-\omega_{bK}}, \tag{31a}$$

taking only the resonance term into account and neglecting the damping. Here, ω_{1sK} is the exciton dispersion:

$$\omega_{1sK}=\omega_{1s0}+\frac{\hbar^2K^2}{2m}. \tag{31b}$$

In uniform bulk materials, $\varepsilon_{\rm pc}$ should be the same as ε_a, the dielectric constant of CuCl, and neglecting the second term in Eq. (31a) gives the photonic dispersion in bulk material without resonance. Therefore, it seems natural to use for $\varepsilon_{\rm pc}$ the dielectric constant computed from the photonic band (dashed line in Fig. 4), when we investigate the bulk properties of polaritons in periodic systems. Next, the bulk exciton dispersion [Eq. (31b)] does not suit our purpose. This is because we have to observe the size-d-quantized exciton levels through the window of the BZ with period l. A simple check suggests that we should renormalize K in Eq. (31b) by a factor of l/d in order to reproduce in the exciton levels at every BZ edge.[17] This K normalization is equivalent to normalizing the mass m by $(d/l)^2$. The dash-dotted line in Fig. 8(a) is the bulk exciton dispersion obtained using the mass $(d/l)^2m=2.02m_0$. Using the $\varepsilon_{\rm pc}$ value and the above exciton dispersion, we computed the polariton dispersion in terms of Eq. (31a) [see the broken line in Fig. 8(a)]. This curve demonstrates an excellent agreement with the energy values of small polariton bands at the edge of every BZ. The same calculation was carried out for sample B (Fig. 9) using the mass $(d/l)^2m=0.98m_0$. The calculation for sample B also reproduces the polariton band edge to a certain degree. The coincidence, however, is not better than for sample A, in particular near the energy region where the exciton-photon coupling is stronger. This appears to result from the weakening of the nonlocality because of the thinner sample B slab, which, however must be studied in more detail. These results are similar to what occurs in the electronic bands of semiconductor superlattices.[15] These small bands can thus found be interpreted as the bands which the lower branch of bulk polariton dispersion has split into due to the coherent interference of the polaritonic waves in the periodic systems.

Now that the lower branch of the polariton is obtained in the form mentioned above, its counterpart, i.e., the upper branch, must also show up in the energy dispersion. This can be discovered in the higher-energy region in Fig. 4, which is replotted as Fig. 8(b). The broken line in Fig. 8(b) represents the upper branch of bulk polariton calculated by the same procedure used for the lower branch. This line exactly repro-

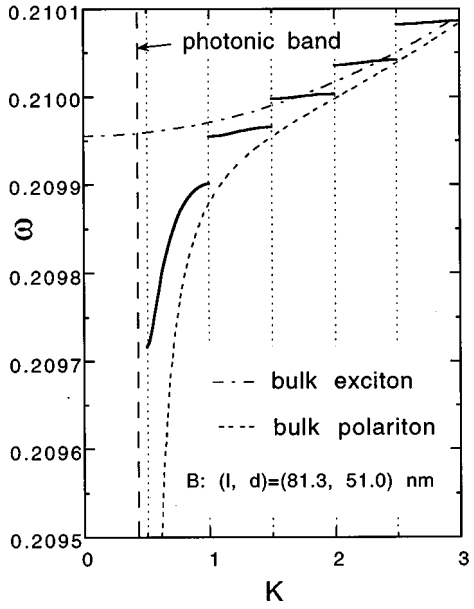

FIG. 9. Polariton dispersion replotted from Fig. 5.

duces the line for the anticrossings. This implies that the anticrossing phenomena are caused by the coupling of the size-quantized exciton states with the upper branch of the bulk polariton. Since the upper branch is already a result of the exciton-photon coupling, the phenomena can be regarded as the product of the sequentially occurring double exciton-photon coupling. The behavior of the polariton dispersion shown in Figs. 8 and 9 entirely results from the excitonic nonlocality and the structural periodicity. If the exciton in the slab were treated as an assembly of local oscillators with the resonance energies of size-quantized states, the photon would couple with each oscillator separately; the resulting polariton dispersion would be merely the sum of the independent polariton dispersions for every oscillator. This point will be discussed further in Sec. IV B.

Next, in Fig. 10 we show the in-depth profiles of the electric field $E_x(z)$ (dotted lines) and the exciton polarization $P_x(z)$ (solid lines) at several typical points of the polariton dispersion for sample A (Fig. 8). The abscissa is normalized in the unit of l. Since these profiles were calculated with the electromagnetic energy fixed in the crystal, the relative strength of $E_x(z)$ and $P_x(z)$ can be compared between different points [10(a), 10(b), 10(c), etc.]. As could be easily predicted, the $P_x(z)$ component is much weaker than $E_x(z)$ at point a (photonlike point) and it increases gradually as it moves along the dispersion curve toward point 10(d). This is evidently caused by the transition of the primary component of the polariton from the photon to the exciton. A more detailed examination shows that the polarization is exactly proportional to the photon field at point 10(a). This tendency, however, gradually diminishes as the excitonic character of the polariton fades in. At point 10(e), the fine structure of the polarization appears to be completely determined by the form of the exciton wave function ($n=14$), regardless of the photon field. This is a natural result of the nonlocal treatment of the exciton, which we recognize by checking the nonlocal

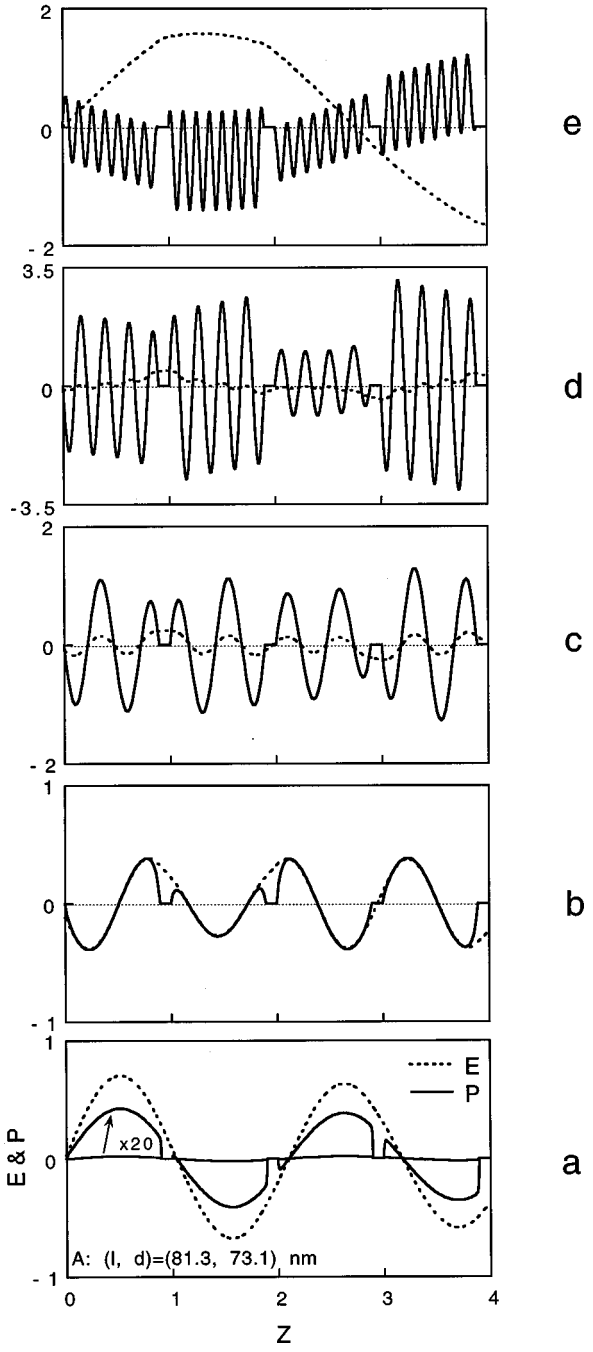

FIG. 10. In-depth profiles of the electric field (dotted lines) and the exciton polarization (solid lines) at several typical points of the polariton dispersion for sample A (Fig. 8). The abscissa is normalized in the unit of l.

polarizability [Eq. (7a)]. At intermediate points 10(b), 10(c), and 10(d), we clearly observe a gradual change of the dominance from photonic to excitonic.

The group velocity of the polariton calculated from the dispersion curve for sample A is shown in Fig. 11. Here v_g is normalized in the unit of light velocity c. The peaks and the valleys of v_g in this figure correspond to photonlike and excitonlike components, respectively, of polaritons. Since the v_g value for the photonic crystal (i.e., neglecting the exciton) is estimated at about 0.44, the polariton group velocity calculated is extraordinarily smaller. In the absence of

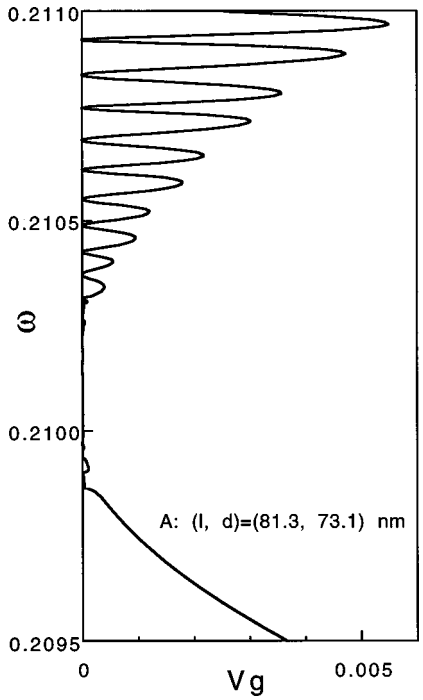

FIG. 11. Group velocity of the polariton calculated from the dispersion curve for sample A. Here, v_g is normalized in the unit of the light velocity c.

light, all exciton bands are dispersionless, i.e., $v_g=0$, which can be easily shown by applying the Bloch theorem to the periodic exciton system without the photon. Therefore, the following probably inaccurate but intuitively understandable interpretation may be possible: the excitons at rest are accelerated by photons while the photons are decelerated by excitons.

B. Long-wavelength approximation

Here, we calculate the polariton dispersions using the long-wavelength (LW) approximation. We select samples A and C as wide and narrow slabs, respectively, for this purpose, i.e., to investigate the applicability of this approximation. The results for sample A are shown in Fig. 12 (solid lines). The dispersion is greatly magnified near the resonance to closely display the fine structures observed just below the $n=0$ exciton level. The dotted line indicates the accurate nonlocal result (replotted from Fig. 4). We see from this figure that LW approximation is not a good approximation for sample A. The lowest two bands (solid lines) are quantitatively very different from those obtained by the accurate method (dotted lines), though they show similar variations. Note that a number of extra small bands separated by small band gaps appear just below the $n=0$ exciton level in the LW approximation, which did not show up in the nonlocal result. This kind of fine structure is also found in higher-energy regions (not shown here): there is a series of small bands converging on every exciton level of even indices ($n=0,2,4,...$). There are no exciton-photon coupled states for odd indices ($n=1,3,5,...$), because of the selection rule deduced from this approximation [Eq. (19b)]. Different from the nonlocal result (see the discussion of Fig. 4), we can specify the locations of discrete exciton levels as the converging points of the series in this approximation. These results may be interpreted as follows. First, for light with longer wavelength, the exciton states behave like the local oscillators with discrete energy levels. The photon coupled with these dispersionless states creates a polariton. This polariton dispersion, however, must split into a number of small bands in the presence of the structural periodicity. The small bands thus produced are zone folded to make a series in Fig. 12. At any rate, the LW approximation cannot reproduce the accurate nonlocal results for samples with this slab thickness.

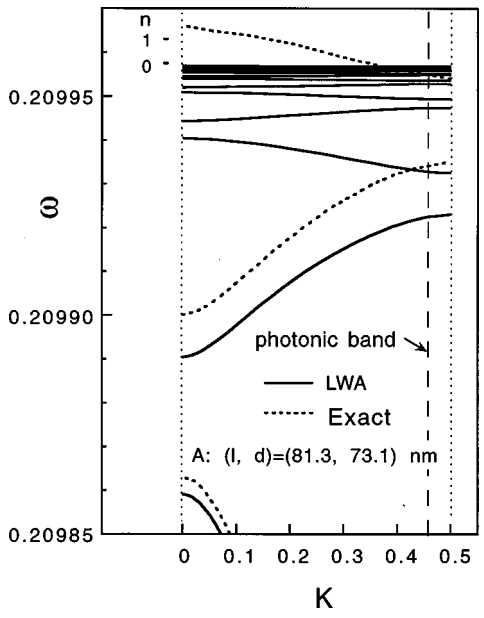

FIG. 12. Polariton dispersion calculated for sample A (with a wide slab) using the long-wavelength approximation. The dotted line indicates the accurate nonlocal result (Fig. 4).

The results for the narrower slab (sample C) are shown in Fig. 13. The overall behavior is almost the same as the nonlocal behavior in Fig. 6: the two results agree completely and therefore only the results for the LW approximation are shown here. There are a couple of differences between them, however. First, extra small bands showed up just below the $n=0$ exciton level. Second, several anticrossings disappeared with this approximation. Both of these phenomena occur for the same reasons mentioned in the discussion of Fig. 12. If we disregard the above discrepancies, the LW approximation can be considered as a good approximation for a sample with this small slab thickness. We know that the parameters for sample C ($l=81.3$ nm, $d=10$ nm, $\lambda=230$ nm, and $a_b=0.7$ nm) satisfy the conditions given by Eq. (16). The criteria intuitively given for the LW approximation to hold are thus verified to be true by the practical problem.

C. Optical response

In this subsection, we demonstrate for our periodic systems the optical responses (absorbance and reflectance) calculated using the method described in Sec. III D. For this purpose, we select sample A as a typical example of the system in which the exciton resonance exists in the photonic band, and sample D as an example of the one whose exciton resonance falls on the photonic band gap.

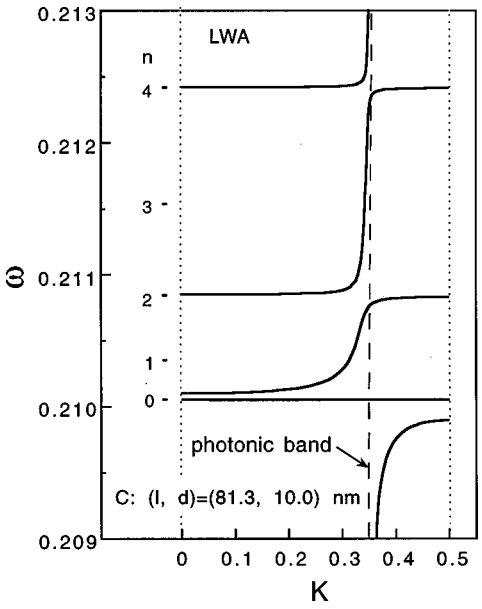

FIG. 13. Polariton dispersion calculated for sample C (with a narrow slab) using the long-wavelength approximation. The main parts of the accurate nonlocal result (Fig. 6) coincide with this approximate result.

For sample A, we display optical responses at three energy regions in separate figures for clarity, focusing on the regions around the exciton resonance (ω_{1s}), the longitudinal-exciton level ($\omega_{1s}+\Delta_{\mathrm{LT}}$), and the higher ($n \gg 1$) size-quantized exciton levels. Figure 14 shows the absorbance and the reflectance around ω_{1s}. The solid lines indicate the results obtained using the total number of unit cells $N=100$ and the dotted lines for one layer ($N=1$). The long tics depicted with the index n show the positions of the lower polariton (LP) energy at the size-quantized wave numbers. The position for $n=0$ is beyond the scope of this figure. The absorbance spectrum for $N=1$ is magnified by a factor of 10. We find a series of the energy regions with the reflectance close to unity. This indicates that no optical modes can exist in the crystal at these energy ranges, and therefore these ranges are regarded as the polaritonic band gaps. Evidently, these ranges show no optical absorption. In contrast, we observe optical absorption due to the formation of small bands in the remaining energy ranges. Since no such phenomenon occurs for $N=1$, this is evidently caused by the periodic structure. We have thus recognized the formation of the polaritonic bands, although true continuous bands are not formed in some regions for the number of unit cells used here ($N=100$). When we compare the results for $N=100$ and $N=1$, it appears that the peaks observed for $N=1$ extend toward the higher-energy side as N is increased, and finally form the bands. The LP positions do not coincide with the absorbance peaks for one layer ($N=1$). This discrepancy occurs because the upper polariton (UP) is mixed into the actual polaritonic wave as an evanescent wave. In fact, the calculation neglecting the UP branch was found to exactly reproduce the absorbance peaks at LP positions. The results shown in Fig. 14 coincide very well with the polariton dispersions discussed earlier (Figs. 4 and 8) quantitatively as well as qualitatively. The above discussion reconfirms the

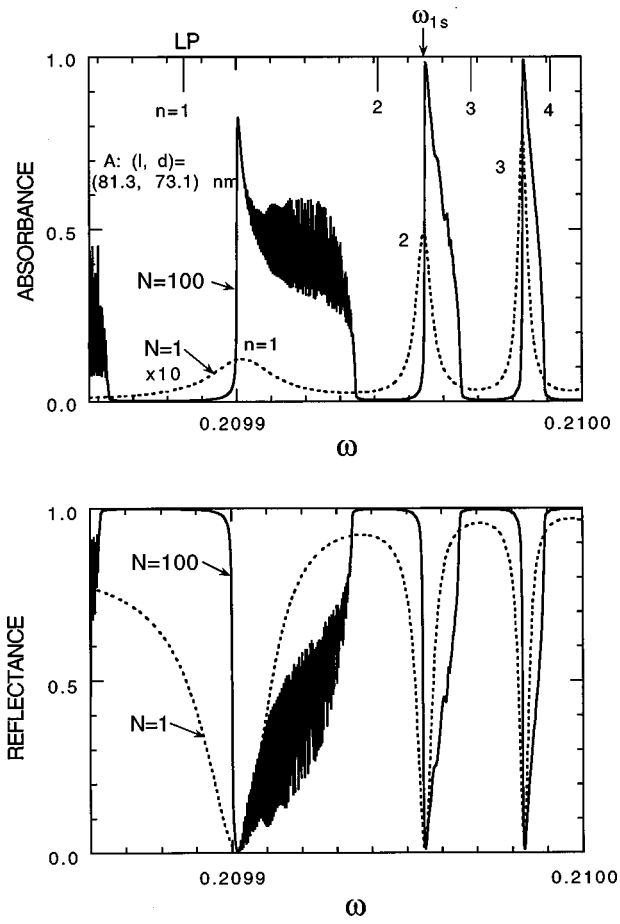

FIG. 14. Absorbance and reflectance spectra for sample A around the exciton resonance (ω_{1s}). Here, and in Figs. 15, 16, and 17, the solid lines are the results obtained using the total number of unit cells $N=100$ and the broken lines are for one layer ($N=1$). The long tics depicted with the index n show the positions of the lower polariton (LP) energy at the size-quantized wave numbers.

interpretation that the bulk polariton dispersion splits into several small bands because of the periodicity of the structure.

Next, let us briefly check the spectra in other energy ranges. Figure 15 shows the absorbance and the reflectance spectra around $\omega_{1s}+\Delta_{\mathrm{LT}}$. The spectra near the longitudinal-exciton resonance are somewhat complicated, because anticrossing (polariton coupling) occurs in this region as well as the band formation. This complexity obscures the band formation. The polariton coupling is more clearly demonstrated in the spectra near the higher exciton levels, an example of which is shown in Fig. 16 for $n=18$. As discussed above, the size-quantized exciton states with higher indices can be regarded as a local oscillator with an isolated well-defined energy level. The spectra in Fig. 16 appear to show the band splitting by the coupling of the local oscillator of $n=18$ with the upper branch of bulk polaritons. The small valley between the two absorption peaks could be regarded as what we call the polaritonic LT (longitudinal-transverse) splitting for the local oscillator $n=18$.

Finally, we show in Fig. 17 the optical response for sample D, in which the exciton resonance exists within the photonic band gap. Evidently, if exciton effects are neglected, there must exist no optical modes in this crystal for

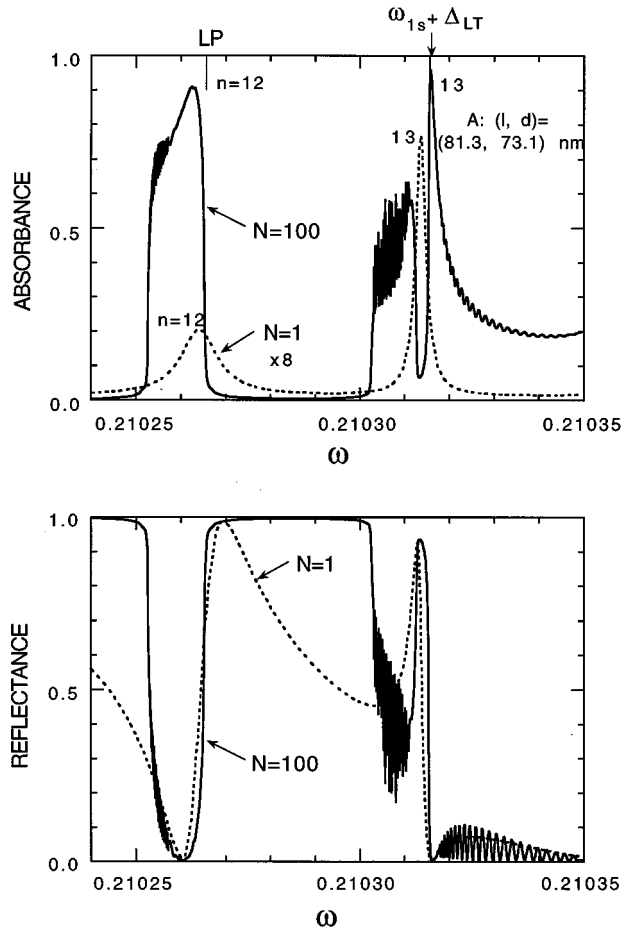

FIG. 15. Absorbance and reflectance spectra for sample A around the longitudinal-exciton state ($\omega_{1s}+\Delta_{LT}$).

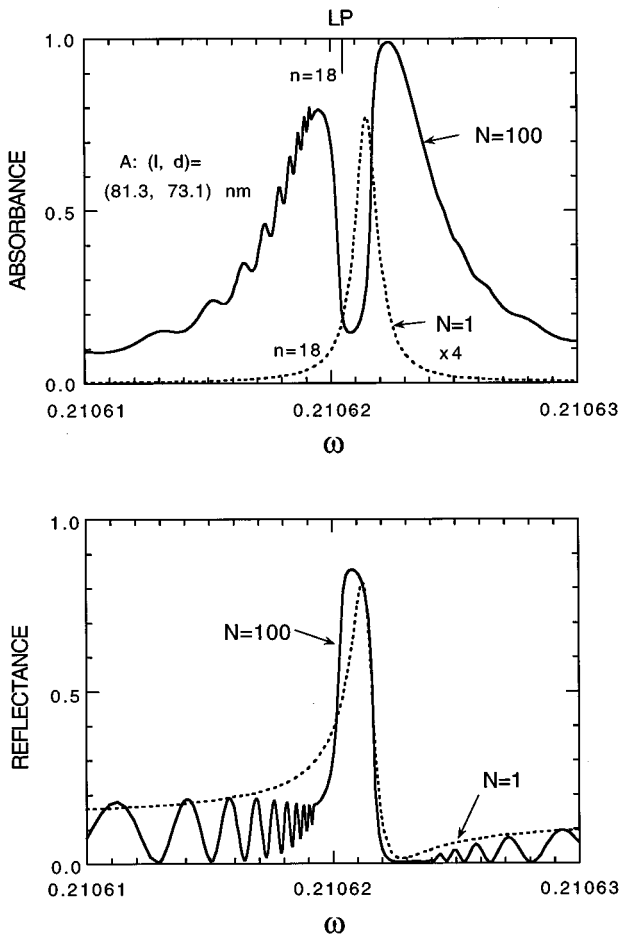

FIG. 16. Absorbance and reflectance spectra for sample A around the higher ($n \gg 1$) size-quantized exciton level.

the energy range shown in the figure. Noteworthy here is that some absorptive structures show up in the spectra by introducing the exciton-photon coupling effects into this crystal. Moreover, the spectra observed are essentially no different from those for sample A. The similar fact was described before in Sec. III A, where the polariton bands were found to be formed for sample D in the photonic band gap. The above results lead to a discussion of the exciton-photon coupling scheme in periodic systems.

Possible coupling schemes in the present system are (i) (photon plus exciton) plus periodicity, (ii) (exciton plus periodicity) plus photon, and (iii) (periodicity plus photon) plus exciton, where (*a* plus *b*) plus *c* implies that *a* and *b* couple first followed by the coupling with *c*. This classification is valid when the coupling of one pair (*a*-*b*) is much stronger than the other two (*b*-*c* and *c*-*a*). Among these coupling schemes, (iii) may be ruled out because it requires us to first build the photonic band and then couple it with an exciton. As discussed in the preceding paragraph, despite the fact that there is not a photon (i.e., the counterpart in the coupling) near the exciton resonance in sample D, we observed polariton bands and absorptions in this energy region. Therefore, the coupling scheme must be different from (iii). Our interpretations for Figs. 3–5 are entirely based on scheme (i), and seem to be valid. As mentioned, the bulk polariton is first created as a result of a strong coupling between a photon and an exciton and then its dispersion splits into bands by the subsequent coupling with the periodicity. This is exactly an analog of the miniband formation in semiconductor superlattices.[15] What differs between the two? Needless to say, one treats electrons while the other treats excitons. In superlattices, the phenomenon is caused by electronic tunneling through thin barriers with finite potential heights. This tunneling can be regarded as a *glue* that connects electronic states in different sites. Since we consider a hard wall, the tunneling of excitons never occurs. The glue in our case is undoubtedly the photon. The phenomenon may be intuitively explained as follows: the photon, which is coupled to an exciton in one slab, modifies its field by this coupling; it propagates to the neighboring slab; it couples again with an exciton in this slab; and so on. The exciton in a slab thus couples with the exciton in a different slab via the photon. The situation may be made clearer if we begin with darkness (very low optical density). In darkness, coupling scheme (ii) holds. The exciton shows constant discrete energy levels (instead of bands) at any *K* value. Therefore, the group velocity is zero and the exciton is localized in each slab. When the light is switched on, scheme (ii) does not hold any more because of the presence of photons and scheme (i) takes over, producing the energy dispersions shown before. The final states thus attained indicate that the exciton component localized in each slab in darkness could be construed as being delocalized with the assistance of the photon.

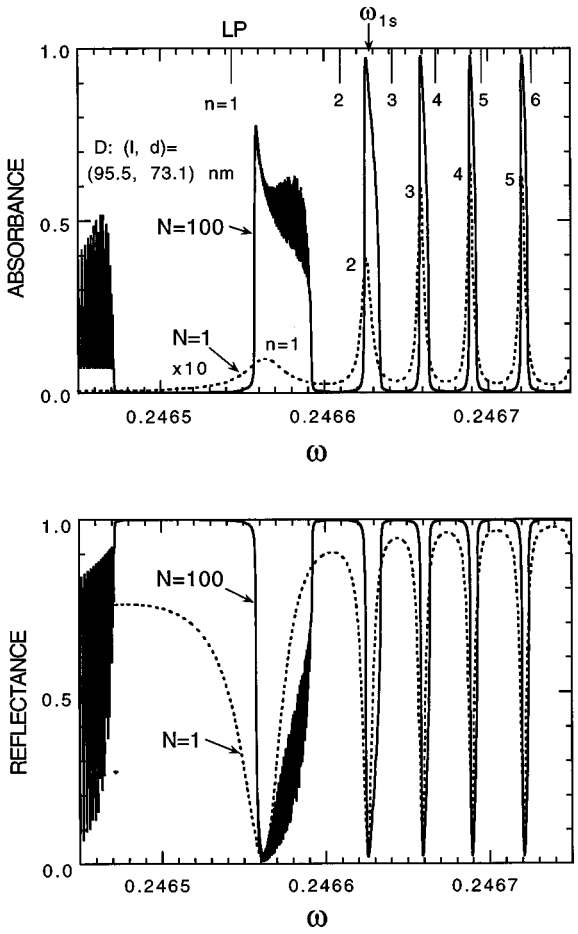

FIG. 17. Absorbance and reflectance spectra for sample D around the exciton resonance (ω_{1s}).

V. CONCLUSION

A theory has been presented for the polaritons (the exciton-photon coupled states) in the periodic structures of dielectric medium (photonic crystals). Treating the excitons in the CuCl lattice points by nonlocal theory, we have clarified the kinetics of excitonic polaritons, which is exhibited in the whole system of one-dimensionally arranged CuCl/NaCl quantum slabs. The results are summarized as follows.

(1) The monotonic energy dispersion in photonic crystal (i.e., neglecting exciton effects) is found to change into an assembly of many small bands separated by small band gaps as a result of introducing exciton effects. The polariton dispersions thus produced show very different behavior among samples with different CuCl slab thicknesses, in particular, near the exciton resonance, indicating the nonlocality of the exciton.

(2) The above polariton dispersion is interpreted as being produced by the splitting of the bulk lower-polariton dispersion in the presence of the structural periodicity. The counterpart of this, i.e., the upper polariton dispersion, anticrosses the discrete exciton levels lying at the higher-energy side. This phenomenon can be regarded as double exciton-photon coupling.

(3) The group velocity of light is shown to be greatly reduced in the presence of excitons. The polarization in-depth profiles have a form reflecting the exciton wave function, because of the excitonic nonlocality.

(4) The long-wavelength approximation is found to be a good approximation for the sample with the CuCl slab thickness of $d=10\,\mathrm{nm}$, whereas it is not the one with $d=73.1\,\mathrm{nm}$. However, this approximation produces a number of extra small bands converging on the exciton level, because it assumes a uniform electric field in the slab.

(5) The absorption and reflectance spectra calculated using the transfer matrices exactly agree with the polariton dispersions mentioned in (1) and (2) above. Two kinds of absorption spectra are observed due to (i) the bands formed by the structural periodicity, and (ii) the exciton levels split due to the coupling between the exciton and the upper polariton branch.

(6) The results for the sample where the exciton resonance is in the photonic band gap suggests that the exciton-photon coupling is much stronger than photon-periodicity and periodicity-exciton couplings.

(7) As a result, in the present periodic systems, the exciton component localized in each slab in darkness could be construed as being delocalized with the assistance of the photon.

APPENDIX A: ANALYTICAL EVALUATION OF SERIES [EQS. (7a) AND (20b)]

The summation in Eq. (7a) was evaluated elsewhere using the integration in the complex K plane. Here, we give a more straightforward way to evaluate it. This summation (denoted S_1) can be modified to

$$S_1=\sum_{n=1}^{\infty}\frac{\sin\frac{\pi nz}{d}\sin\frac{\pi nz'}{d}}{n^2+a^2}$$
$$=m\left(\frac{d}{\pi\hbar}\right)^2\left[f_a\left(\frac{\pi}{d}(z'-z)\right)-f_a\left(\frac{\pi}{d}(z'+z)\right)\right], \quad \text{(A1)}$$

where we replaced $n+1$ by n, and the function $f_a(x)$ is defined by

$$f_a(x)=\sum_{n=1}^{\infty}\frac{\cos nx}{n^2+a^2}. \quad \text{(A2)}$$

This series is known to have an analytical form[18]

$$f_a(x)=\frac{\pi}{2a}\frac{\cosh a(\pi-x)}{\sinh a\pi}-\frac{1}{2a^2} \quad \text{(A3)}$$

for $0<x<2\pi$. Since $0<z,\ z'<d$, then $0<(\pi/d)(z'+z)<2\pi$ and $-\pi<(\pi/d)(z'-z)<\pi$. Hence, formula (A3) can be used to calculate $f_a((\pi/d)(z'+z))$. On the other hand, the above formula can also be used to calculate $f_a((\pi/d)(z'-z))$ by replacing its argument by $(\pi/d)|z'-z|$, because $0<(\pi/d)|z'-z|<\pi$. This replacement does not change the result. We thus obtain the analytical expression for the polarization in Eq. (8).

The summation given by Eq. (20b) (denoted S_2) can be rewritten as

$$S_2=\sum_{n=1,3,\ldots}^{\infty}\frac{\sin nx}{(n^2+b^2)n}, \quad \text{(A4)}$$

replacing $n+1$ by n, where $x=(\pi/d)u$ and hence $0<x<\pi$. Here the summation must be carried out for odd n. Since we focus on $\mathbf{K}_{\|}=0$, then a defined in Eq. (7b) is the same as b defined in Eq. (20c). Consider a function defined by

$$F_b(x)\equiv\int_0^x dx\, f_b(x), \tag{A5}$$

where $f_b(x)$ is given by replacing b with a in Eq. (A2). Since $0<x<\pi$ for x in Eq. (A4), this condition falls within the requirement $0<x<2\pi$ for formula (A3) to hold. This integration gives a formula

$$F_b(x)=\sum_{n=1}^{\infty}\frac{\sin nx}{(n^2+b^2)n}=\frac{\pi}{2b^2}\left[1-\frac{\sinh b(\pi-x)}{\sinh b\pi}\right]-\frac{x}{2b^2}. \tag{A6}$$

Here we used $F_b(0)=0$. Then S_2 can be obtained by subtracting the two series

$$S_2=\sum_{n=1}^{\infty}\frac{\sin nx}{(n^2+b^2)n}-\sum_{n=2,4,\ldots}^{\infty}\frac{\sin nx}{(n^2+b^2)n}$$

$$=F_b(x)-\frac{1}{8}F_{b/2}(2x). \tag{A7}$$

The second series in Eq. (A7) was evaluated by changing n by $2n'$ $(n'=1,2,3,\ldots)$ and using Eq. (A6). Since $0<2x<2\pi$, the formula of Eq. (A3) can be used to calculate $F_{b/2}(2x)$. The formula obtained for S_2 gives the function $H_b(x)$ in Eq. (21).

APPENDIX B: BLOCH THEOREM FOR INTEGRODIFFERENTIAL EQUATION

Here we demonstrate, by the group-theoretic approach,[19] that the Bloch theorem can be applied to the operator including the integral operator described by

$$H=\frac{d^2}{dz^2}+\alpha(z)+\int_{-\infty}^{\infty}dz'\beta(z,z') \tag{B1}$$

under some kind of spatial periodicity for the coefficients $\alpha(z)$ and $\beta(z,z')$. Here, needless to say, the integral operator in Eq. (B1)—when it operates onto a function $\varphi(z)$—implies integration over z' after taking this function as $\varphi(z')$ into its integrand. We introduce a translation operator T_n by

$$T_n\varphi(z)\equiv\varphi(z+nl). \tag{B2}$$

Our problem is equivalent to the problem of whether or not T_n always commutates with H:

$$[T_n,H]=0. \tag{B3}$$

Then, we compute the commutator for a function $\varphi(z)$,

$$[T_n,H]\varphi(z)=\alpha(z+nl)\varphi(z+nl)-\alpha(z)\varphi(z+nl)+\int_{-\infty}^{\infty}dz'\beta(z+nl,z')\varphi(z')-\int_{-\infty}^{\infty}dz'\beta(z,z')\varphi(z'+nl). \tag{B4}$$

By replacing the variable z' by $z'+nl$ in the first integral in Eq. (B4), we obtain

$$[T_n,H]\varphi(z)=[\alpha(z+nl)-\alpha(z)]\varphi(z+nl)+\int_{-\infty}^{\infty}dz'[\beta(z+nl,z'+nl)-\beta(z,z')]\varphi(z'+nl). \tag{B5}$$

Since the background dielectric constant term $\alpha(z)$ is periodic in our system, this part evidently commutates with T_n. Under the periodicity we imposed intuitively before on the kernel $\beta(z,z')$ [Eqs. (10a) and (10b)], the second term in Eq. (B5) evidently vanishes. Therefore, our assumption for the kernel's periodicity supports the existence of the Bloch-type wave function. Noteworthy here is that one of our intuitive assumptions [Eq. (10a)] is unnecessary to satisfy the Bloch theorem. In other words, the Bloch theorem holds only if

$$\alpha(z+nl)=\alpha(z)\quad\text{and}\quad\beta(z+nl,z'+nl)=\beta(z,z') \tag{B6}$$

for any combinations of z and z' in the periodic structures. These conditions permit us to treat the system, in which the nonlocality extends to other slabs (neighboring and next neighboring slabs, etc.).

APPENDIX C: TRANSFER MATRICES

$$M_s=\frac{1}{2}\begin{pmatrix}1+q_0q_b^{-1} & 1-q_0q_b^{-1}\\ (1-q_0q_b^{-1})e^{-iq_b(l-d)} & (1+q_0q_b^{-1})e^{-iq_b(l-d)}\end{pmatrix}, \tag{C1}$$

$$M_g=\frac{1}{2}\begin{pmatrix}(1+q_0q_b^{-1})e^{-iq_b(l-d)} & \\ 1-q_0q_b^{-1} & \end{pmatrix}, \tag{C2}$$

and

$$M_t=\begin{pmatrix} 1 & e^{iq_b(l-d)} \\ q_b & -q_b e^{iq_b(l-d)} \end{pmatrix}^{-1} \begin{pmatrix} e^{iQ_1 d} & e^{iQ_2 d} & 1 & 1 \\ Q_1 e^{iQ_1 d} & Q_2 e^{iQ_2 d} & -Q_1 & -Q_2 \end{pmatrix}$$
$$\times \begin{pmatrix} (Q_1^2-q^2)^{-1} & (Q_2^2-q^2)^{-1} & (Q_1^2-q^2)^{-1}e^{iQ_1 d} & (Q_2^2-q^2)^{-1}e^{iQ_2 d} \\ (Q_1^2-q^2)^{-1}e^{iQ_1 d} & (Q_2^2-q^2)^{-1}e^{iQ_2 d} & (Q_1^2-q^2)^{-1} & (Q_2^2-q^2)^{-1} \\ 1 & 1 & e^{iQ_1 d} & e^{iQ_2 d} \\ Q_1 & Q_2 & -Q_1 e^{iQ_1 d} & -Q_2 e^{iQ_2 d} \end{pmatrix}^{-1} \begin{pmatrix} 0 & 0 \\ 0 & 0 \\ e^{iq_b(l-d)} & 1 \\ q_b e^{iq_b(l-d)} & -q_b \end{pmatrix}. \tag{C3}$$

[1] *Nanostructures and Quantum Effects*, edited by H. Sakaki and H. Noge (Springer-Verlag, Heidelberg, 1994).

[2] E. Yablonovich and T. J. Gmitter, Phys. Rev. Lett. **63**, 1950 (1989).

[3] E. Yablonovich, Phys. Rev. Lett. **58**, 2059 (1987).

[4] *Photonic Band Gaps and Localization*, edited by C. M. Soukoulis (Plenum, New York, 1993).

[5] S. Nojima, Jpn. J. Appl. Phys. **37**, L565 (1998).

[6] S. Nojima, Jpn. J. Appl. Phys. **37**, 6418 (1998).

[7] S. Nojima, Phys. Rev. B **57**, 2057 (1998).

[8] L. Belleguie and S. Mukamel, Phys. Rev. B **52**, 1936 (1995).

[9] D. S. Citrin, Solid State Commun. **89**, 139 (1994).

[10] R. Zeyher, J. L. Birman, and W. Brenig, Phys. Rev. B **6**, 4613 (1972).

[11] A. D'Andrea and R. Del Sole, Phys. Rev. B **25**, 3714 (1982).

[12] K. Cho and M. Kawata, J. Phys. Soc. Jpn. **54**, 4431 (1985).

[13] C. Weisbuch and R. G. Ulbrich, in *Light Scattering in Solids III*, edited by M. Cardona and G. Guntherodt (Springer-Verlag, Berlin, 1982), p. 218.

[14] S. I. Pekar, Zh. Eksp. Teor. Fiz. **33**, 1022 (1957) [Sov. Phys. JETP **6**, 785 (1958)].

[15] L. Esaki and R. Tsu, IBM J. Res. Dev. **14**, 61 (1970).

[16] H. Haug and S. W. Koch, *Quantum Theory of the Optical and Electronic Properties of Semiconductors* (World Scientific, Singapore, 1990), p. 207.

[17] There is a mistake in the discussion leading to the *m* renormalization in Ref. 7. The discussion in the present paper is correct.

[18] A. P. Prudinkov, Yu. A. Brychkov, and O. I. Marichev, *Integrals and Series* (Gordon & Breach, New York, 1986).

[19] C. Kittel, *Quantum Theory of Solids* (J. Wiley, New York, 1963).